Estimation of geostrophic current in the Red Sea based on Sea level anomalies derived from extended satellite altimetry data

Ahmed Mohammed Taqi[a,b], Abdullah Mohammed Al-Subhi[a], Mohammed Ali Alsaafani[a] and Cheriyeri Poyil Abdulla[a]

[a]Department of Marine Physics, King Abdulaziz University, Jeddah, Saudi Arabia;

[b]Department of Marine Physics, Hodeihah University, Hodeihah, Yemen

Correspondence to: Ahmed. M. Taqi (ataqi@stu.kau.edu.sa)

Abstract

The geostrophic currents data near the coast of the Red Sea has large gaps. Due to this, the sea level anomaly (SLA) data of Jason-2 has been reprocessed and extended towards the coast of the Red Sea and merged with AVISO data at the offshore region. This processing has been applied to build a gridded data to achieve best results for the SLA and geostrophic current. The results obtained from the new extended data at the coast are more consistent with the observed data (CTD) and hence geostrophic current calculation. The pattern of SLA distribution and geostrophic currents are divided into two seasons; winter (October – May) and summer (June – September). The geostrophic currents in summer are flowing northward except the eastern coast which flows in the opposite. In winter, currents flow to the north for the entire sea except a small part of the eastern coast (22°N-24°N). This flow is modified with the presence of the cyclonic and anticyclonic eddies, which are more concentrated in the central and northern Red Sea. The results show anticyclonic eddies (AE) on the eastern side of the Red Sea and cyclonic eddies (CE) on the western side during winter. In summer, cyclonic eddies are more dominant for the entire Red Sea while in winter both cyclonic and anticyclonic eddies are present. The result shows a change in some eddies from anticyclonic during winter to cyclonic during summer in the north between 26.3°N –27.5°N. Furthermore, the lifespan of cyclonic eddies is longer than that of anticyclonic eddies.

1. Introduction

The Red Sea is a narrow semi-enclosed water body that lies between continents of Asia and Africa. It is located between latitude 12.5°-30°N and longitude 32°E-44°E in an NW-SE orientation. Its average width is 220 km and the average depth is 524 m (Patzert, 1974). It is connected at its northern end with the Mediterranean Sea through the Suez Canal and at its southern end with the Indian Ocean through the strait of Bab El- Mandab. The exchange of water through Bab El- Mandab (shallow sill of 137 m) is the most significant factor that determines the oceanographic properties of the Red Sea (Smeed, 2004).

During winter, the southern part of the Red Sea is subject to SE monsoon wind, which is relatively strong from October to December, with a speed of 6.7-9.3 ms^{-1} (Patzert, 1974). During the summer season, the wind is shifting its direction to be from NW. On the other hand, in the northern part of the Red Sea, the dominant wind is NW all year around.

The circulation in the Red Sea is driven by strong thermohaline and wind forces (Neumann and McGill, 1961; Phillips, 1966; Quadfasel and Baudner, 1993; Siedler, 1969; Tragou and Garrett, 1997). Several studies in the Red Sea have focused on thermohaline circulation, where they found that the exchange flow between the Red Sea and Gulf of Aden consists of two layers in winter and three layers in summer through Bab El- Mandab (e.g.Phillips 1966; Tragou and Garrett 1997; Murray and Johns 1997; S. Sofianos and Johns 2015;Al Saafani and Shenoi, 2004; Smeed, 2004). Other studies describe the basin-scale circulation based on modelling approach, usually forced at a relatively low-resolution (1°x1°) by buoyancy flux and global wind (Clifford et al., 1997; Sofianos, 2003; Tragou and Garrett, 1997; Biton et al., 2008; Yao et al., 2014a,b). The horizontal circulation in the Red Sea consists of several eddies, some of them are semi-permanent eddies (Quadfasel and Baudner, 1993), that often present during the winter (Clifford et al., 1997; Sofianos and Johns, 2007) in the northern Red Sea. The circulation system in the central Red Sea is dominated by cyclonic (CE) and anticyclonic eddies (AE), mostly between 18°Nand 24°N. Eddies are also found in the southern Red Sea but not in a continuous pattern (Johns et al., 1999). Zhan et al., (2014) reported recurring or persistent eddies in the north and the central Red Sea, although there are differences in the number of eddies, their location, and type of vorticity (cyclonic or anticyclonic).

The long-term sea level variability in the Red Sea is largely affected by the wind stress and the combined impact of evaporation and water exchange across the strait of Bab El Mandeb (Edwards, 1987; Sultan et al., 1996). The Sea level in the Red Sea is higher during winter and lower during summer (Edwards, 1987; Sofianos and Johns, 2001; Manasrah et al., 2004). It is characterized by two cycles, annual and semi-annual, where the annual cycle is dominant (Abdallah and Eid, 1989; Sultan and Elghribi, 2003).

In recent years, there has been an increasing interest for using satellite altimetry Sea level anomaly (SLA) which offer large coverage and long data period for providing measurements of SSH, wave height and wind speed (Chelton et al., 2001). However, the altimeter data undergoes several processing stages for corrections due to the atmosphere and ocean effects (Chelton et al., 2001). The satellite altimetric data has been used for the open ocean for a long time with great success, while the data of the coastal region suffers from gaps of almost 50 km form the coastline. The coastal region requires further corrections due to additional difficulties based on the closeness of the land (Deng et al., 2001; Vignudelli et al., 2005; Desportes et al., 2007; Durand et al., 2009; Birol et al., 2010). In the past two decades, many researchers have sought to develop different methods to improve the quality, accuracy and availability of altimetric data near the coast (e.g. Vignudelli et al., 2000; Deng and Featherstone, 2006; Hwang et al., 2006; Guo et al. 2009, 2010; Vignudelli et al., 2005; Desportes et al., 2007; Durand et al., 2009; Birol et al., 2010; Khaki et al., 2014; Ghosh et al., 2015; Taqi et al., 2017). The satellite altimetry faces three types of problems near the coast; (1) the echo interference with the surrounding ground as well as the inland water surface reflection (Andersen and Knudsen, 2000; Mantripp, 1966), (2) environmental and geophysical corrections such as dry tropospheric correction, wave height, high frequency and tidal corrections from global models, etc. and (3) spatial and temporal corrections during sampling (Birol et al., 2010).

The ocean currents circulate water worldwide. They have significant influence on the transfer of energy and moisture between the ocean and the atmosphere. Ocean currents play a significant role in climate change in general. In addition, they contribute to the distribution of hydrological characteristics, nutrients, contaminants and other dissolved materials between the coastal and the open areas, and among the adjacent coastal regions. Ocean currents carry sediment from and to the coasts, so play a significant role in shaping of the coasts. That is

90   important in the coastal region where in the densely inhabited coastal region, producing large

91   amounts of pollutants. Understanding of the currents helps us in dealing with the pollutants and

92   coastal management.

93   The objective of the present research is to study the geostrophic current in the Red Sea

94   including the coastal region using the modified along track Jason-2 SLA along the coast produced

95   by Taqi et al., (2017).

2. Material and Methods

2.1. Description of data

2.1.1 Fourier series model (FSM) SLA

99   The SLA data used in this study is weekly Jason-2 along the track from June 2009 (cycle

100   33) to October 2014 (cycle 232) which has been extended to the coastal region by Taqi et al.,

101   (2017). To cover all the period, additional tracks were added up to December 2014 (cycle 239).

102   The extended data shows a good agreement with the coastal tide gauge station data. In brief, the

103   FSM method of extending SLA consists of four steps; the first step is the removal from SLA the

104   outliers which are outside three times standard deviation from mean. Second step; the SLA is

105   recomputed using Fourier series equation along the track. Third step; the data is then filtered to

106   remove the outliers in the SLA with time similar to the first step. Finally, the SLA data is linearly

107   interpolated over the time to form the new extended data which is called FSM. For more details

108   on the FSM method, refer to Taqi et al., (2017).

2.1.2 AVISO, Tide Gauge, and hydrographic datasets

110   This study uses two types of SLA data; The first set is the (SLA), which has been

111   downloaded from the Archiving Validation and Interpretation of Satellite Oceanographic (AVISO)

112   (ftp://ftp.aviso.altimetry.fr/global/delayed-time/grids/msla/all-sat-merged). The second dataset is

113   the SLA from the extended FSM data. The temperature and salinity profiles used for geostrophic

114   estimation are received from three cruises, the first cruise was during March 16 to 29, 2010

115   onboard R/V Aegaeo between 22°N to 28°N along the eastern Red Sea with a total of 111

116   Conductivity, Temperature and Depth (CTD) profiles. For more details; see Bower and Farrar

117   (2015). The second cruise was on April 3 to 7, 2011 onboard Poseidon between 17°N to 22°N in

118   the central eastern Red Sea and the third one was during October 16 to 19, 2011 onboard the same

119   vessel between 19°N to 23°N in the central eastern Red Sea as a part of Jeddah transect, KAU-

120   KEIL Project. For more details; consult R/V POSEIDON cruise P408/1 report (Schmidt et al.,

121   2011). The availability of in-situ observations is limited in space and time because of the spatial

122   and temporal distribution of the available cruises. Finally, three tide gauges data at the eastern

123   coastline of the Red Sea are obtained from the General Commission of Survey (SGS) at the

124   Kingdom of Saudi Arabia (Fig.1) and their location details are shown in Table 1.

125   2.2 Method

126   The SLA data used in this study are coming from two sources: (1) the FSM data near the

127   coast and (2) the AVISO data along the axis of the Red Sea. The steps to merge the two datasets

128   and calculating the geostrophic currents are given below.

129   First, the along-track FSM data are used to produce gridded data to a spatial resolution of

130    $0.25° \times 0.25°$ for the comparison with Aviso data. In the second step, AVISO data near the coast

131   is removed, and replaced with the coastal FSM gridded data leaving space between the two data

132   set according to the width of the sea either one or two grid cells. This gap was filled using kriging

133   interpolation method to smooth the dataset. The merged data hereafter called as FSM-SLA.

134   Finally, surface geostrophic currents are estimated from FSM-SLA data using the following

135   equation;

$$136 \qquad u_g = -\frac{g}{f}\frac{\partial \zeta}{\partial y} \qquad\qquad v_g = \frac{g}{f}\frac{\partial \zeta}{\partial x} \qquad (1)$$

137   Where (u_g, v_g) is the surface geostrophic current, g is gravity, f is the Coriolis parameter and ζ is

138   the sea surface height. The estimation of geostrophic currents from CTD data is using the following

139   equation;

$$140 \qquad u_g = -\frac{1}{f\rho}\frac{\partial p}{\partial y} \qquad\qquad v_g = \frac{1}{f\rho}\frac{\partial p}{\partial x} \qquad (2)$$

141   where ρ is the density of seawater, p is hydrostatic pressure derived from the density. The stations

142   have depths that very from 50 up to 2344 m. However, most of the stations (~90 %) exceed the

143   500 m depth. Previous study by Quadfasel and Baudner (1993) used 400 m as level of no motion

144   to calculate geostrophic current in the Red Sea. Based on ADCP measurements, Bower and Farrar

145   (2015) shown that, on average, 75–95 % of the vertical shear is occurred over the top 200 m of the

146   water column. Moreover, the ADCP measurements of current speed below 500 m is very small;

147   about ~0.06m/s at 600 m depth (Bower and Farrar, 2015). Therefore, expecting negligible

148   variability below 500 m, a depth of 500 m was selected as a level of no motion. We have compared

149 the geostrophic current corresponding to level of no motion at 500m and 700m. The observed

150 difference between both are negligibly small.

151 Table 1. The location of tide gauge stations and period of measurement.

Station	Latitude	Longitude	Period
Jazan	16.87	42.55	1/1/2013 to 31/12/2013
Jeddah	21.42	39.15	1/1/2013 to 31/12/2013
Yanbu	23.95	38.25	1/1/2013 to 31/12/2013

152
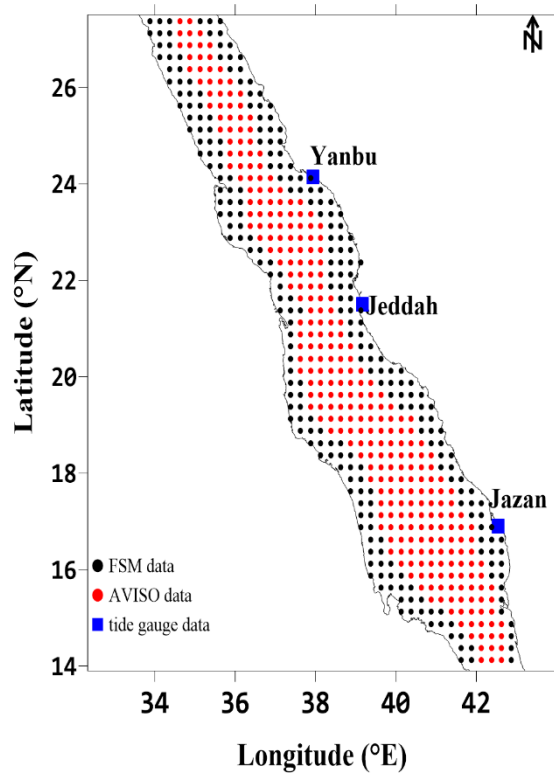
153 Figure 1. show the study area and the grid-points locations with a spatial resolution of 0.25° ×

154 0.25° and locations of the tide gauges.

3. Result and Discussion

3.1 Validation of FSM-SLA and geostrophic current

157   The statistical analysis has been conducted to show the quality of FSM-SLA as compared

158 with AVISO. The Correlation Coefficient (CC) reveals a good agreement between the two datasets

159   in the open sea (about 0.7 to 0.9) and is shown in Fig. 2. Near the coasts, on the other hands, shows

160   weak correlation coefficient between the two data sets; 0.45 to 0.7.

161   Furthermore, the observed SLA from the coastal tide gauge is compared with the FSM-SLA data

162   and AVISO datasets. Table 2. illustrates some of the statistical analysis, where the root mean

163   square error (RMSE) is lower for FSM-SLA as compared to that of AVISO.

164

165   Table 2. statistical analysis for AVISO and FSM-SLA data with observed data (in 2013).

	Jasan		Jeddah		Yanbu	
	FSM-SLA	AVISO	FSM-SLA	AVISO	FSM-SLA	AVISO
CC	0.936	0.914	0.915	0.906	0.907	0.895
RMSE(m)	0.073	0.085	0.069	0.094	0.067	0.104
Note: The p-value corresponding to all comparison is very low (P<0.0001), indicating that the results from correlation are significant.						

166

167
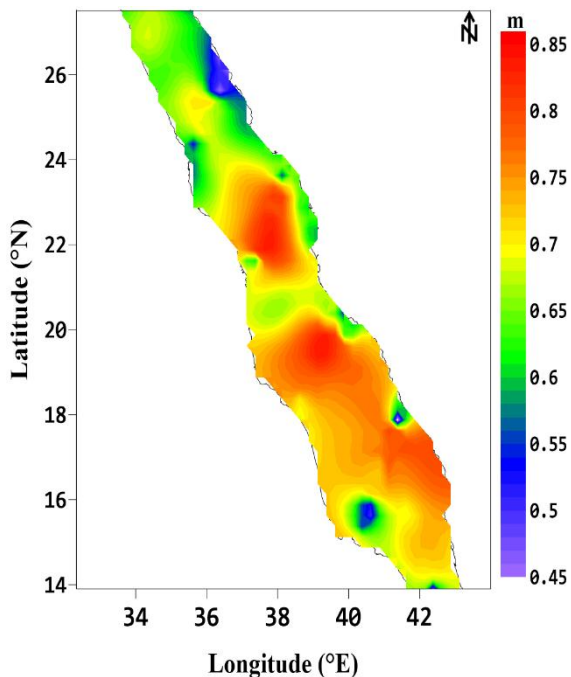
168   Figure 2. show the correlation coefficient between AVISO and FSM data
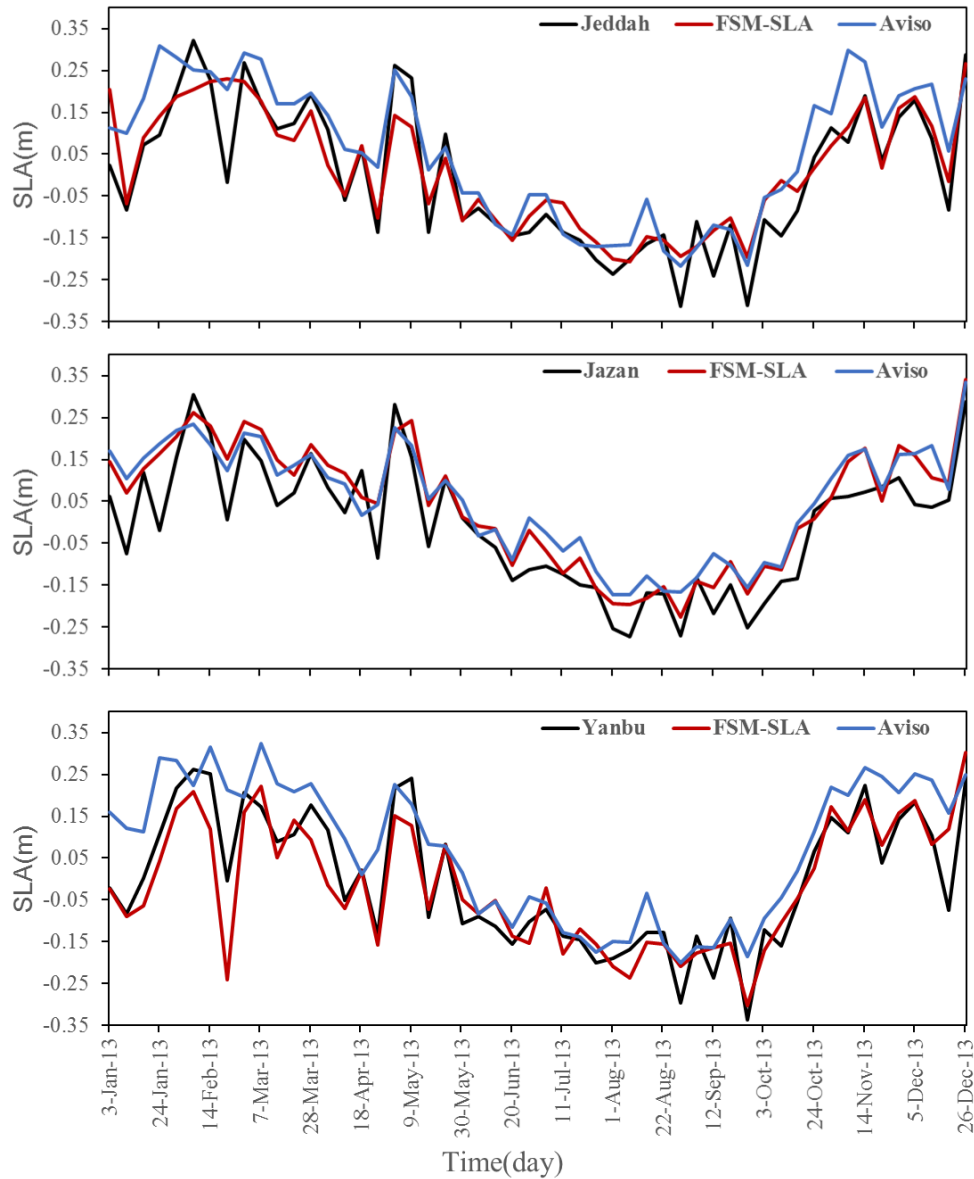
Figure 3. Comparison of SLA from three tide gauge (black), with grid FSM-SLA data (red) and Aviso (blue)

Figure 3 shows the SLA time series for 2013 from the three coastal stations as compared with the FSM-SLA and AVISO. The three stations datasets have similar seasonal pattern and FSM-SLA coincides with observed SLA in shorter-duration fluctuations. This agreement is clearly shown in Table 2. The comparison of FSM-SLA data and the observed SLA data (at Jazan, Jeddah, and Yanbu stations) show a better correlation than between the AVISO and observed SLA data as shown in Fig.3 and Table .2. These correlation coefficient differences indicate that the FSM-SLA

177 shows better accuracy near the coast. These results were consistent with those obtained for along-

178 track Jason-2 SLA with coastal stations by Taqi et al., (2017).

179
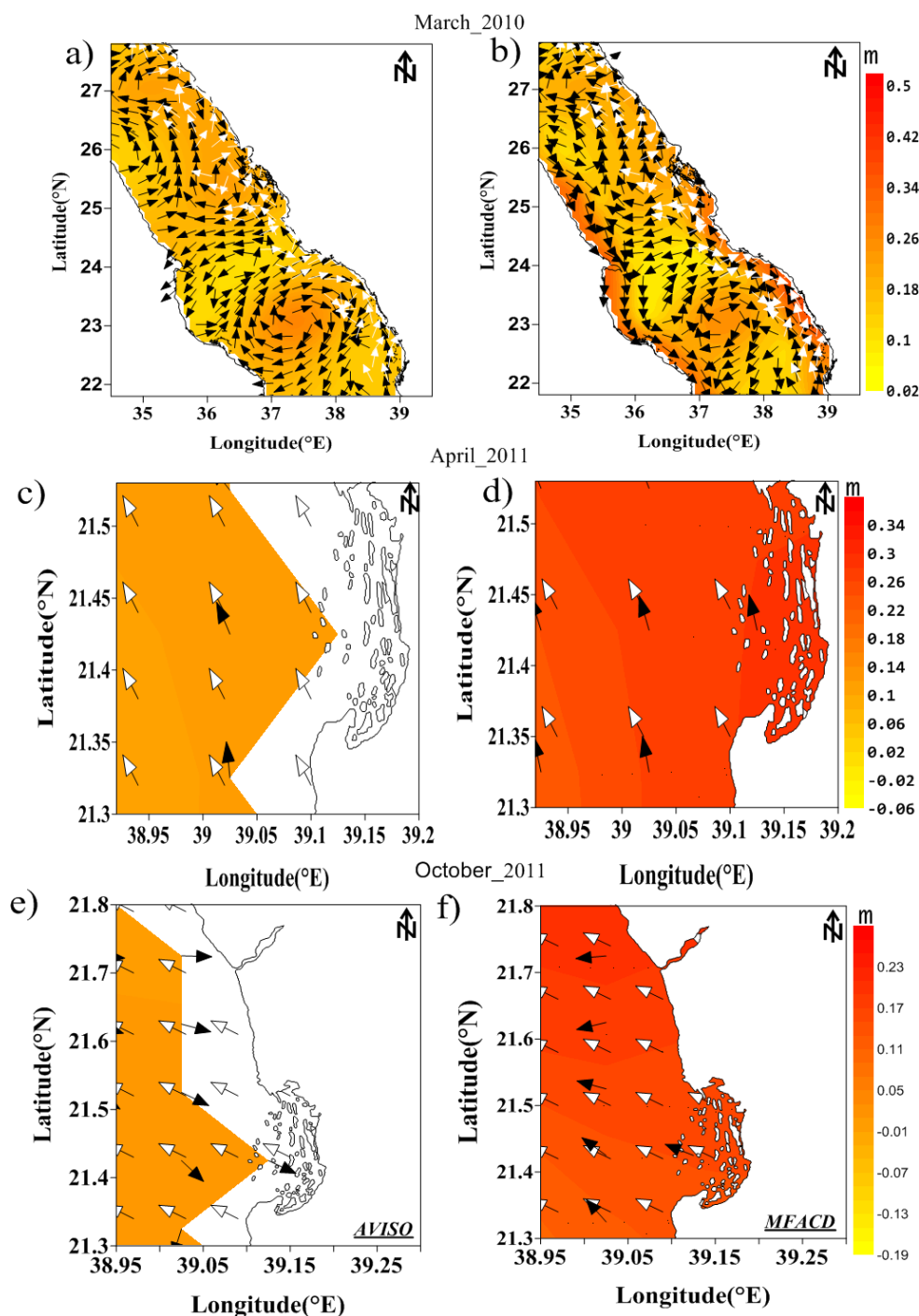
180 Figure 4. Comparison for three months' SLA (color) and geostrophic currents (black vectors)

181 between (left) AVISO and (right) FSM-SLA white vectors show geostrophic currents from CTD

182 data.

183   Figure 4 shows a comparison between the geostrophic currents for the central Red Sea

184 derived from AVISO and FSM-SLA for three different times (March 2010, April 2011, and

185 October 2011), those different periods corresponding to the timing of three cruises described in

186 section 2.1.

187   It can be seen from the Fig. 4(b, d & f) that there is a significant matching in the directions

188 of geostrophic currents from FSM-SLA with CTD data near the coast and offshore. This result is

189 in agreement with Bower and Farrar (2015) findings, especially in October 2011 (Fig. 4f). In

190 March 2010, the geostrophic current near the coast estimated from FSM-SLA is in match with

191 directions of CTD-derived geostrophic current in most regions. However, the directions of

192 geostrophic currents from AVISO are not always in match with CTD-derived one especially in

193 October 2011.

194   In March 2010 the geostrophic currents along the eastern coast of the Red Sea are towards

195 the north for both FSM-SLA and AVISO, except between $22.2° - 23°$N, where the FSM-SLA and

196 CTD data geostrophic currents are in the same direction while AVISO geostrophic current is in

197 the opposite direction (see Fig. 4a,4b).

198 Table 3. statistical analysis for the speed of geostrophic current from FSM-SLA and AVISO

199 compared with CTD-derived geostrophic current from the thress cruises.

		Month-Year	Bias (m/s)	RMSE (m/s)	Stdv (m/s)	CC
current speed	FSM-SLA	Mar-2010	-0.0085	0.065	0.066	0.54
	AVISO		-0.01	0.08	0.08	0.48
	FSM-SLA	Apr-2011	-0.28	0.31	0.15	0.61
	AVISO		-0.87	0.89	0.21	0.44
	FSM-SLA	Oct-2011	-0.19	0.49	0.45	0.53
	AVISO		-0.51	0.70	0.48	0.49

200

201   The speed of geostrophic current data derived from FSM-SLA and CTD during the months

202 (March 2010, April 2011, October 2011) shows a stronger correlation compared with the speed of

203 geostrophic current derived from AVISO and CTD as shown in Fig. 4 and Table 3.

3.2 Description of FSM-SLA and geostrophic current

Figure 5 shows monthly climatology variation for the 6-year period for SLA and geostrophic current. The SLA is higher during the period from October to May and lower during rest of the year, this pattern is consistent with previous studies (Patzert, 1974; Edwards, 1987; Ahmad and Sultan, 1989; Sofianos and Johns, 2001; Sultan and Elghribi, 2003;Manasrah et al., 2004, 2009). Based on calculations made here, the geostrophic current of Red Sea along the eastern coast is northward while along the western coast is southward. This northward flowing current is consistent with a previous study by Bower and Farrar (2015). Similar results are also obtained from three-dimensional modeling by (Clifford et al., 1997; Eshel and Naik, 1997; Sofianos, 2003, 2002). The Fig.5 presents the surface circulation during January in the northern part, where two eddies formed between $25^{o} - 27.5^{o}$N. The first eddy is an anticyclone between $26.3^{o} - 27.5^{o}$N on the eastern side of the Red Sea. The other eddy is cyclonic located between $25^{o} - 26.3^{o}$N near the western coast. To the south of that, there are two other eddies between $22.5^{o} - 24.7^{o}$N, cyclonic on the western side and anticyclonic on the eastern side. These results match those observed in previous studies by (Eladawy et al., 2017; Sofianos and Johns, 2003a). Two cyclonic eddies and an anticyclonic eddy found at $19.5^{o} - 22.5^{o}$N are consistent with those modeled by Sofianos and Johns, (2003). Near Bab al-Mandab, there is a cyclonic eddy on the western side between $15^{o} - 16.5^{o}$N.

In February, the surface circulation of the Red Sea is similar to that during January, with some differences in the eddies structure. The anticyclonic eddy near 27°N on the eastern sides of the Red Sea starts shifting toward the western coast, while a cyclonic eddy at $25^{o} - 26.3^{o}$ N start appearing. The cyclonic eddies between $22.5^{o} - 24.7^{o}$N on the western side are less clear in this month.

In March and April, all the eddies are located along the central axis of the Red Sea. In the north, the anticyclonic eddy near 27°N is shown in both months, while the cyclonic eddy is not clear during March and April. The anticyclonic eddy shown near 23-24°N during March is weakening during April. Also, the anticyclonic eddy between 19-20°N is shrinking during April.

In May, there is no clear eddy between 27.5^{o}N and 25°N. However, four eddies are clearly existing between $19.5^{o} - 25^{o}$N; two cyclonic eddies at $24^{o} - 25^{o}$N, and $20^{o} - 22^{o}$N, two anticyclonic eddies at $23^{o} - 24^{o}$N, and $19.5^{o} - 20^{o}$N. From the previous results, it can be seen several cyclonic

234 and anticyclonic eddies distributed all over the Red Sea and these results match those in modelling

235 studies (Clifford et al., 1997; Eladawy et al., 2017; Sofianos, 2003, 2002, Yao et al., 2014a)

236 During June, the flow of the geostrophic currents in the northern part reversed its direction.

237 This accompanies a formation of large cyclonic eddy extending from $25.5^o - 27.5^oN$ occupying the

238 entire width of the Red Sea. To the south of it, another cyclonic eddy observed between $24^o - 25^oN$

239 and an anticyclonic eddy between $23^o - 24^oN$ are also noticed during June with a similar strength

240 during May. The cyclonic eddy seen between $17^o - 20^oN$ during May, is also seen during this

241 month with more strength. To the south of it, the flow is towards the Bab el-Mandab following

242 normal summer pattern. The flow pattern along the coast is similar to results of (Chen et al., 2014)

243 for winter (January to April). The short-term climatology of geostrophic current in the Red Sea is

244 dominated by cyclonic and anticyclonic eddies all over the Red Sea, and especially in the central

245 and northern parts of the sea.

246 During July-September, the flow of the geostrophic currents structure is similar to that of

247 June with two cyclonic eddies north of 24.5^oN and an anticyclonic eddy between $23^o - 24^oN$. South

248 of these eddies, another cyclonic eddy extends to 19^oN. Furthermore, south of 19^oN, there is an

249 outflow towards the south all over the width of the Red Sea with narrow inflow along the eastern

250 coast of the Red Sea. The Fig. 6 also shows an anticyclonic between $18^°-19^oN$ and a cyclonic

251 between $16^°-17^oN$ during August and September. These results are consistent with the results from

252 previous studies (Clifford et al., 1997; Eladawy et al., 2017; Sofianos, 2003, 2002, Yao et al.,

253 2014b).

254 During summer (June-September), the changes in wind speed and direction cause reversed

255 of changes in the direction of flow consequently, the locations of eddies are also changed (Chen

256 et al., 2014). The surface current flows from the Red Sea to the Gulf of Aden through the Bab-el-

257 Mandeb. The anticyclonic eddy shown in the north at 27.5^oN in winter is replaced with cyclonic

258 eddy, during this season. Summer is dominated by cyclonic eddies as shown in Fig. 6.
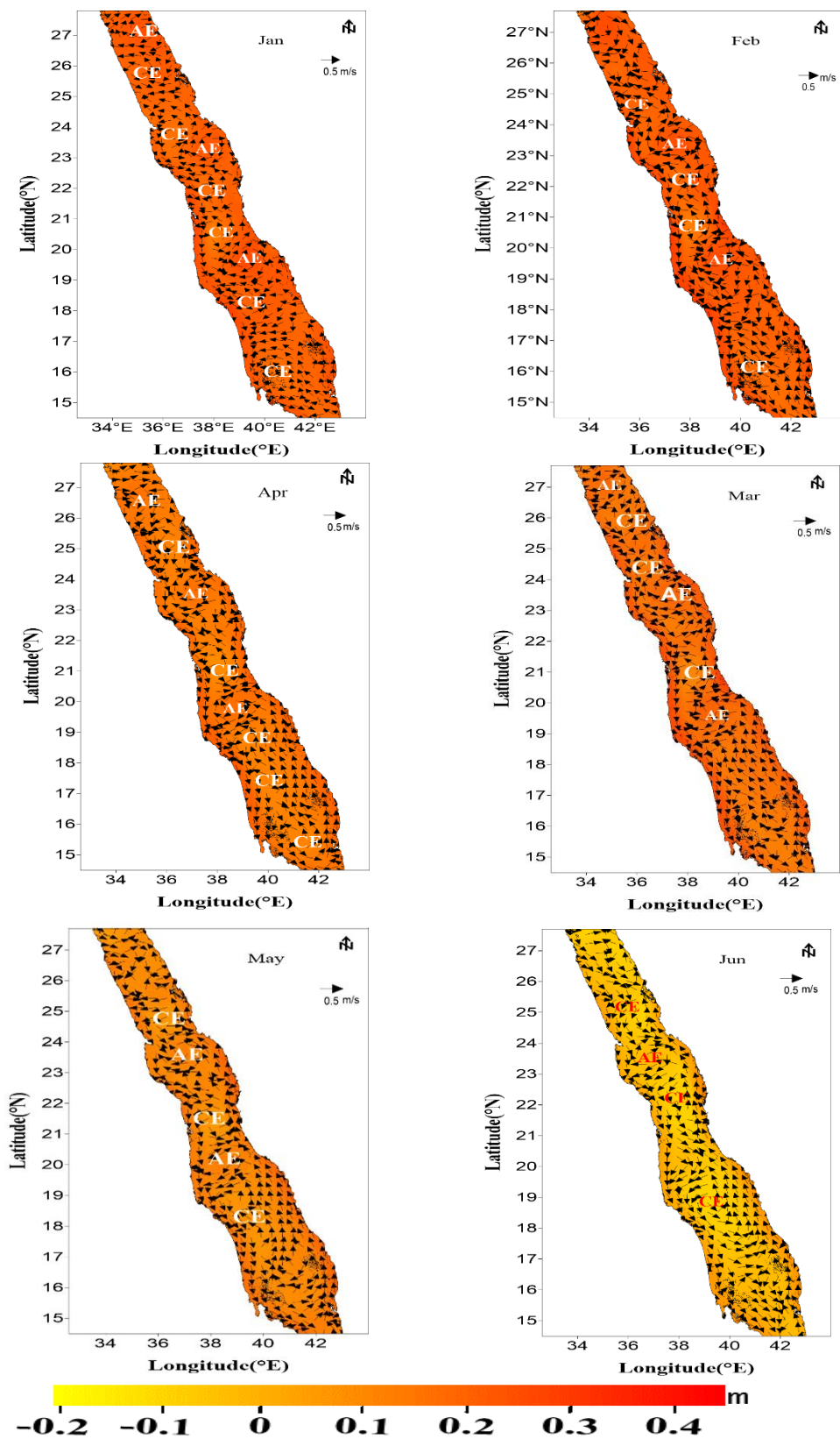
Figure 5. shown monthly climatology for geostrophic current and Sea level anomaly (Reference current length =0.5m/s)
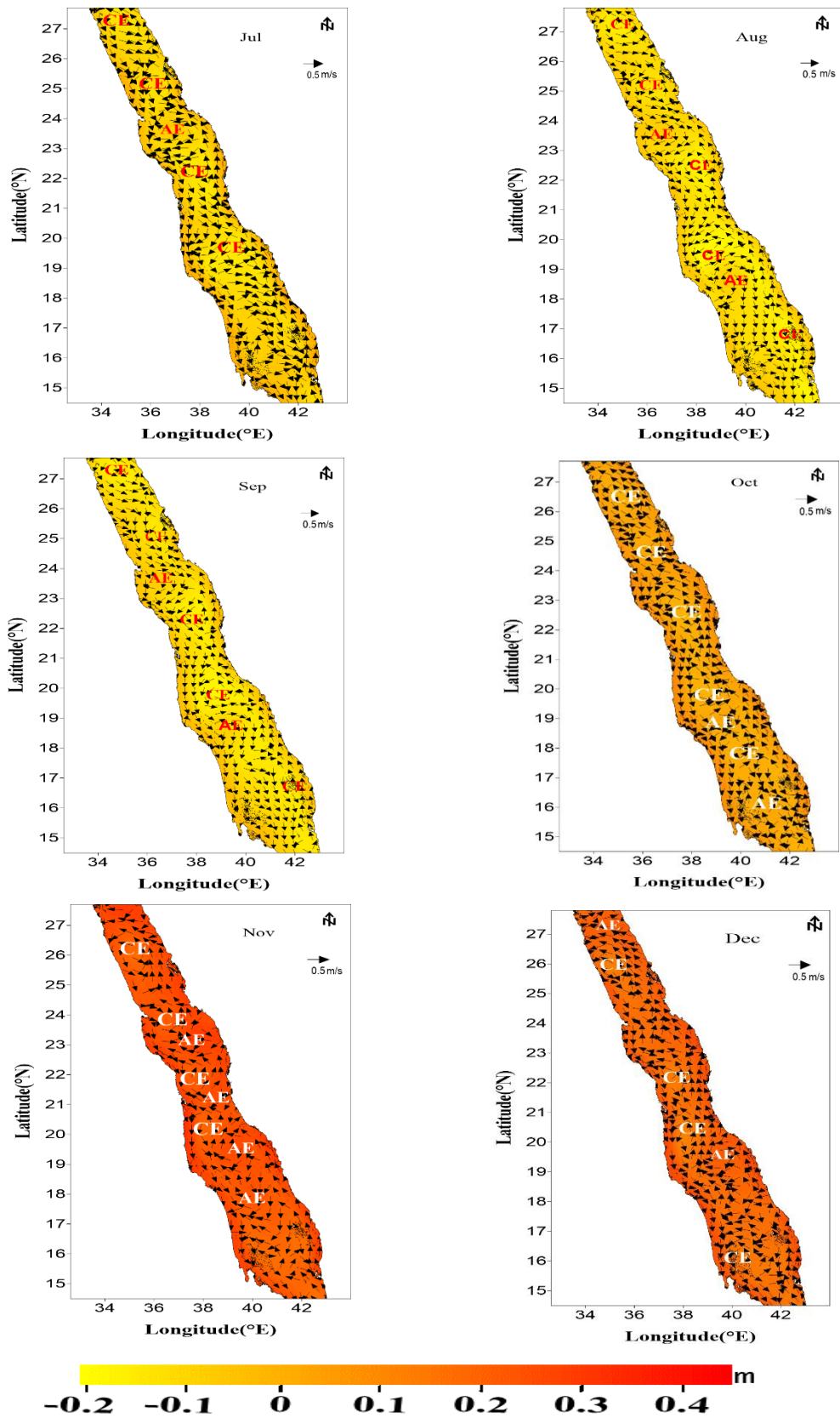
261   Figure 6. As Fig. 5 for July to December

262   During October, the geostrophic current is weak as compared with that during September, still cyclonic but with less strength. The anticyclone seen during September between $23^o - 24^o$N is not clear during October and formation anticyclone eddy between 15°-16^oN. In the central and southern parts, the flow of the geostrophic currents is towards south along the western coast and towards the north along the eastern side with the presence of cyclonic and anticyclonic eddies in the central axis of the Red Sea with a weak flow. In November and December, the structure of geostrophic currents are similar to that of October but with stronger currents and well established cyclonic and anticyclonic eddies.

270   During summer, the cyclonic eddies are often concentrated on the west side and the anticyclonic eddies on the eastern side of the Red Sea, while in winter it is the opposite. Their formation might be related to wind forces and thermohaline (Neumann and McGill, 1961; Phillips, 1966; Quadfasel and Baudner, 1993; Siedler, 1969; Tragou and Garrett, 1997).

274   Since the general circulation in the Red Sea is largely modified with the presence of cyclonic and anticyclonic eddies, the identification of eddies in the study area were conducted based on defining the eddies in terms of SLA (Chelton et al., 2011). Figure 7 shows statistical variability of lifespan, number of eddies, amplitude, and the mean speed of geostrophic current in the center of the eddies with latitude for 6 years. Statistical analysis indicates that eddies are generated over the entire Red Sea, mostly concentrated between $18°$-24^oN, obviously stronger than any other latitude. The amplitude of an eddy has been defined as the differences between the estimated basic height of the eddy boundary and the extremum value of SLA inside the eddy interior parts. The mean amplitude for anticyclonic is between 1.3 cm at southern Red Sea to 5.3 cm at northern Red Sea and for cyclonic eddy is between 1.6 cm at southern Red Sea to 4.2 cm at northern Red Sea. The result indicates the average value of eddy amplitude in the Red Sea (including low latitude and high latitude) is about 4 cm, which is within the reasonable range defined by (Chelton et al., 2011). The average lifespan of the cyclonic eddies is longer than that of the anticyclonic eddies. Moreover, the mean speed of geostrophic current for the entire Red Sea is about 5-10 cm/s, which has reached three-times higher in the $25°$-26^oN latitude band for both cyclonic and anticyclonic. These results match those observed in previous study Zhan et al., (2014).

291
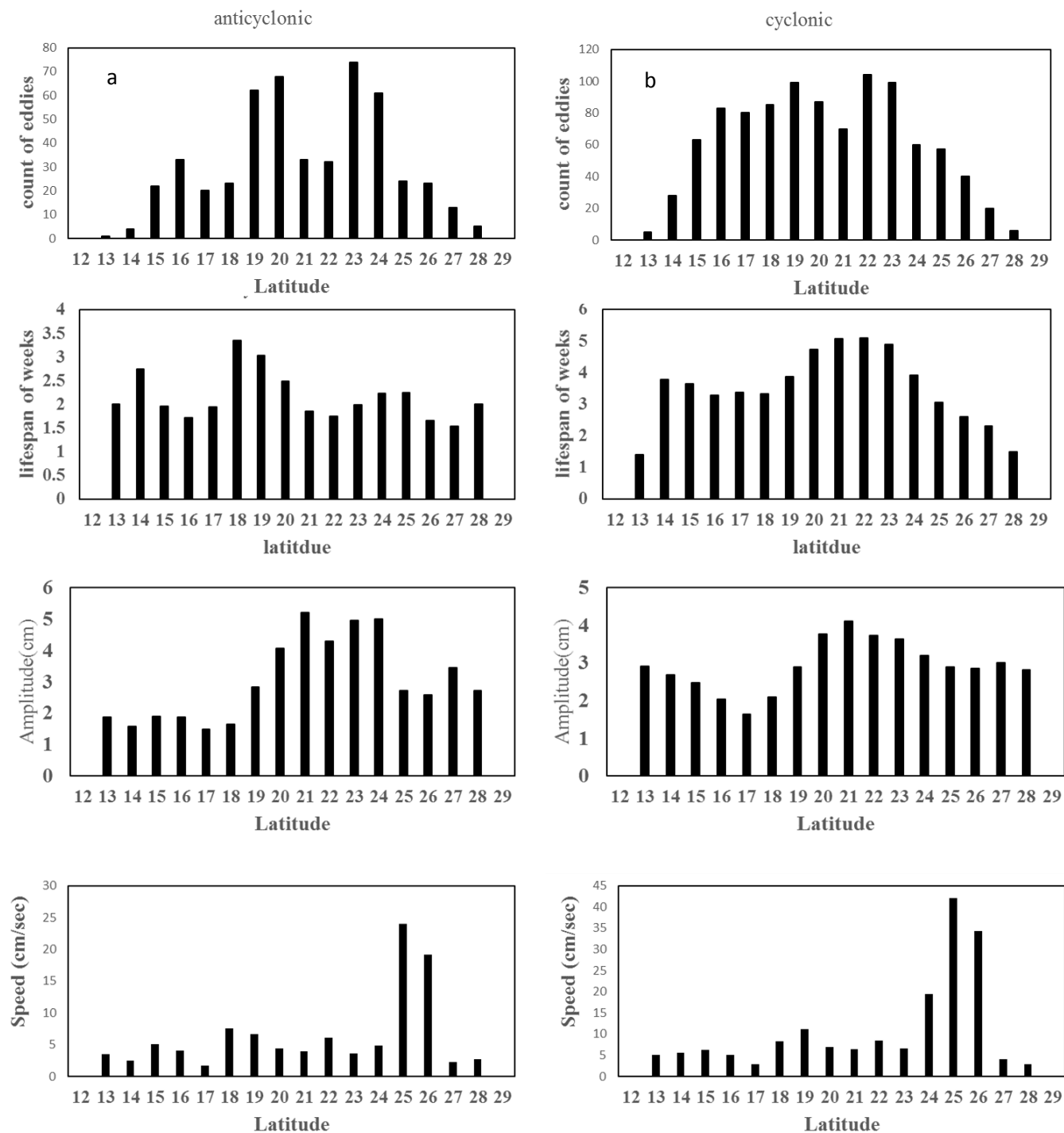
Figure 7. the variability of eddies with latitude for cyclonic (right panel) and anticyclonic (left panel).

294
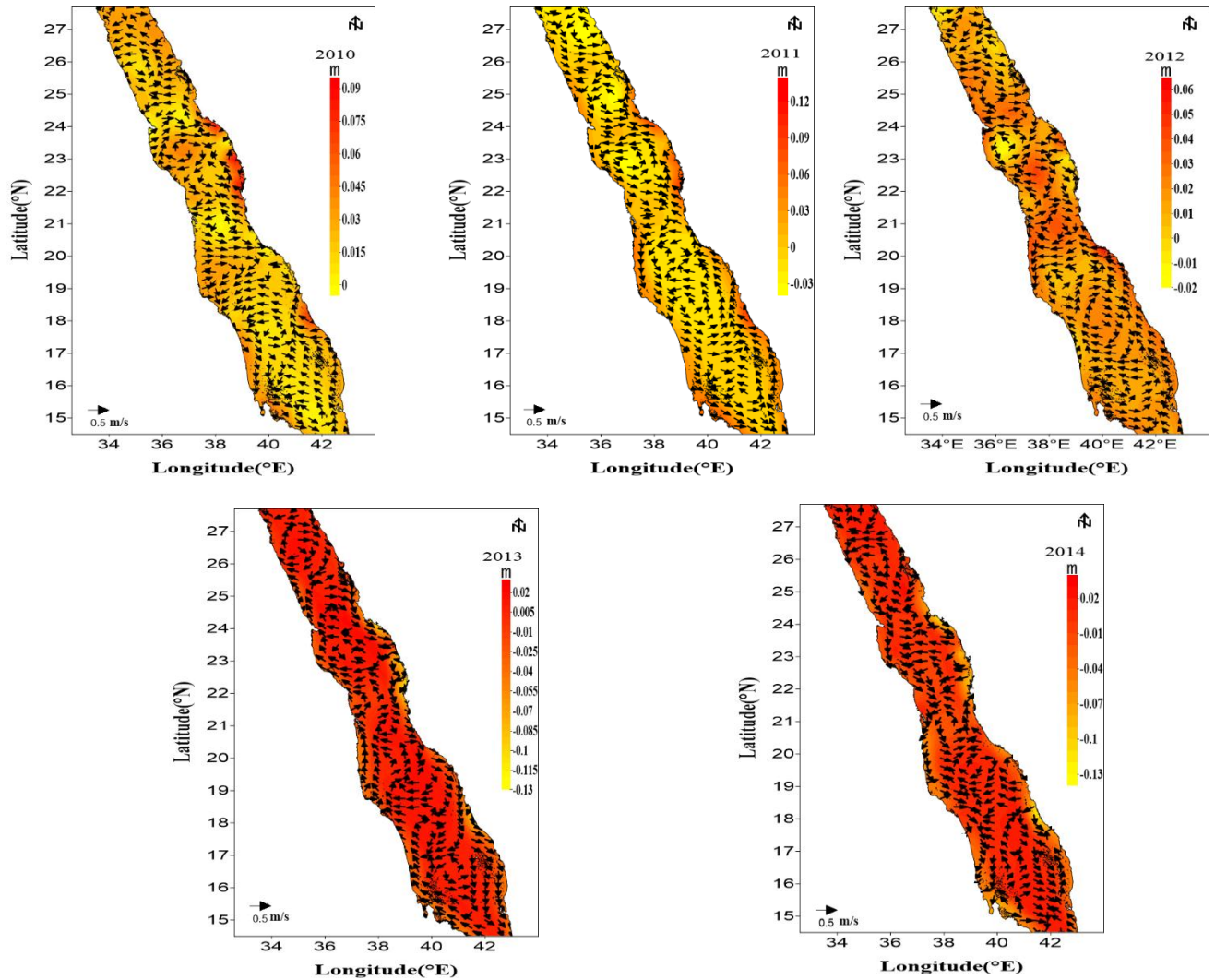
Figure 8. Maps of the annual mean SLA as a deviation from 6-yr mean.

Figure 8 shows the annual mean of SLA as deviation from the 6-year mean. The interannual variability of SLA and geostrophic currents is clearly seen in the southern part of the Red Sea while in the northern part, the pattern is similar for all years except for 2013 where the cyclonic replaced by anticyclonic eddy. The SLA and geostrophic distribution observed during 2011 are similar to that shown in Papadopoulos et al., (2015), with the cyclonic eddy along the eastern side seen more clearly. Moreover, due to extension of our data we could compute the cyclonic pattern up to the coast. The geostrophic currents direction is irregular along the coast, which is northward most of the time. The eddies were mostly concentrated in the north and central parts of the Red Sea.

305   The statistical analysis between annual FSM-SLA with 6-year mean (Table 4) is less

306   biased with lower RMSE value and strong correlation. The standard deviation shows low value

307   for each year.

308   Table 4. Statistical analysis for the annual mean of FSM-SLA compared deviation from 6-yr mean.

Year	Bias	RMSE	STD	CC
2010	-0.009	0.023	0.019	0.544
2011	-0.012	0.029	0.024	0.774
2012	-0.009	0.025	0.022	0.548
2013	-0.013	0.037	0.032	0.791
2014	-0.013	0.036	0.032	0.726

309

310
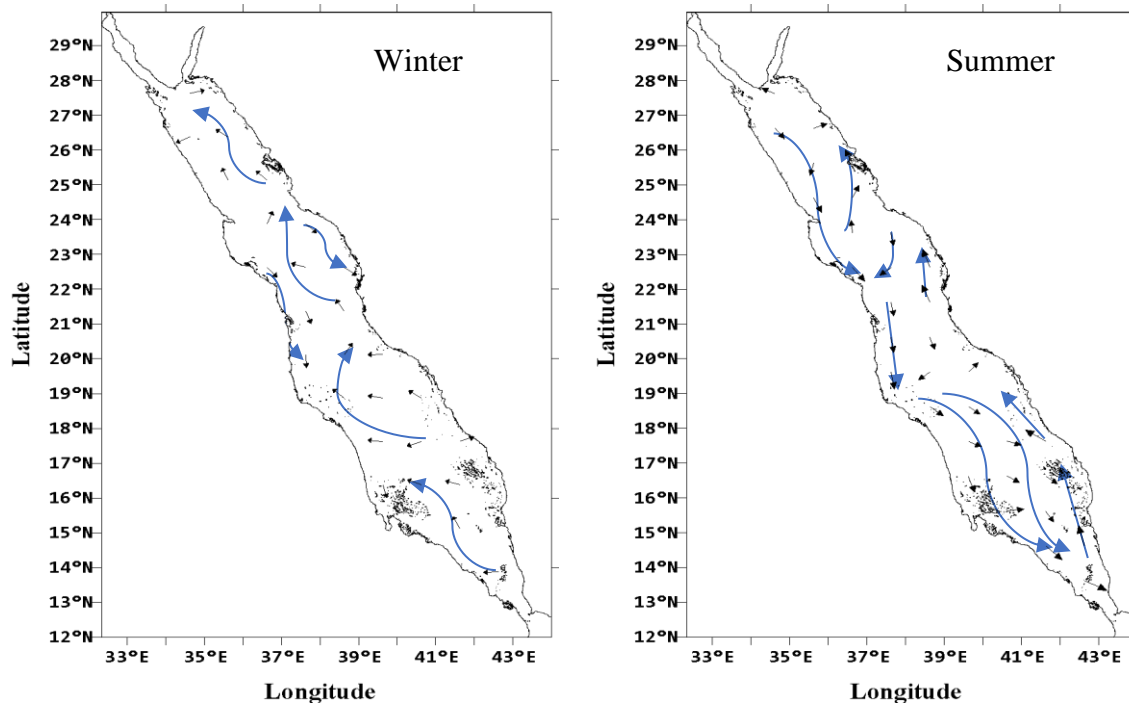
311   Figure 9. Winter and summer seasonal average surface geostrophic currents, black arrows are

312   actual surface geostrophic currents and blue arrows are schematic streamline.

313   Figure 9 shows the general schematic of the seasonal variability of geostrophic currents

314   derived from 6 years. During winter, the mean flow is toward the north mostly along the western

315   coast up to 16°N, this result agrees with Sofianos and Johns, (2003) then it shifts to the eastern

316   coast up to 20°N. The flow is along the middle from 20°N to the north. The mean flow is toward

317 the north mostly along the western coast and center up to 23°N then it shifts to the eastern coast.
318 Apart from this, southward coastal geostrophic currents are observed along the eastern coast
319 (22°N-24°N) and the western coast (23°N-20°N). During summer, the flow is towards the south
320 along the western side of the sea while in the southern part the flow spreads for most of the area
321 of the Red Sea with a narrow northward direction near the eastern coast.

4. Conclusion

323 In general, the geostrophic current has been estimated from FSM-SLA for Red Sea region,
324 and the distribution of the geostrophic current shows that the winter period extends from October
325 to May and summer period extends from June to September. This pattern is similar to that shown
326 by (Sofianos and Johns, 2001). There was a lack in measurements of coastal currents in the Red
327 Sea. This study was able to produce data near the coast. The major new findings from the present
328 study include the monthly geostrophic pattern in the Red Sea which has not been published before.
329 The finding of this paper considered the first of its type in the Red Sea for extending SLA and
330 geostrophic currents to the coast beside giving more details of eddies spatial and temporal
331 variabilities in the coastal region.

332 The southern Red Sea show significant interannual variability in the geostrophic current
333 pattern, while the central and northern parts are negligible difference over the years. The
334 geostrophic along the eastern coast is towards the north while along the western coast of the sea
335 it is southward. Seasonally, the geostrophic currents in summer are flowing northward except the
336 eastern coast which flows in the opposite. In winter, currents flow to the north for the entire sea
337 except small part of the eastern coast (22°N-24°N) and the western coast (23°N-20°N). In this
338 study, northward flowing eastern coastal current during summer is documented for the first time
339 in the Red Sea.

340 The cyclonic eddies were relatively larger than the anticyclonic eddies in the Red Sea. The
341 eddies are concentrated in the central and north of the Red Sea more than the southern side. That
342 the mean amplitude for anticyclonic and cyclonic at lower latitudes has low amplitude and at
343 higher latitudes has high amplitude. In winter, the cyclonic eddies are beside the west coast and
344 anticyclonic eddies on the east side in the Red Sea, while in summer it is the opposite. Also, in
345 some locations there is a noticeable change from anticyclonic during winter to cyclonic during
346 summer and vice versa between 26.3°N –27.5°N. The analysis of the eddies found that during the

347 summer the cyclonic eddies are dominant than winter in the entire Red Sea, while eddies of both
348 polarities observed during winter. The finding of this paper considered the first of its type in the
349 Red Sea for extending SLA and geostrophic currents to the coast beside giving more details of
350 eddies spatial and temporal variabilities in the coastal region.

351 **Acknowledgments**

352 The authors are deeply grateful to the data providers. JPL Physical Oceanography Distribution
353 Active Archive Center (PODAAC), the Archiving Validation and Interpretation of Satellite
354 Oceanographic (AVISO) to provide Jason-2 data. This also extends to the Saudi Arabian GCS for
355 providing hourly tide gauge data along the coast of the Red Sea. They are thankful for the High-
356 Performance Computing center at King Abdulaziz University (http://hpc.kau.edu.sa) for giving us
357 a chance to use their facilities during analyses of data. Our thanks are for King Abdulaziz
358 University, Jeddah, Saudi Arabia and Hodeidah University, Yemen for making this research
359 possible.

360

361 **References**

362 Abdallah, A. M. and Eid, F. M.: On the steric sea level in the Red Sea, Int. Hydrogr. Rev., 66(1),
363 115–124., 1989.
364 Ahmad, F. and Sultan, S. A. R.: On the heat balance terms in the central region of the Red Sea,
365 Deep Sea Res. Part A. Oceanogr. Res. Pap., 34(10), 1757–1760, 1987.
366 Ahmad, F. and Sultan, S. A. R.: Surface heat fluxes and their comparison with the oceanic heat-
367 flow in the red-sea, Oceanol. acta, 12(1), 33–36, 1989.
368 Al Saafani, M. A. and Shenoi, S. S. C.: Seasonal cycle of hydrography in the Bab el Mandab
369 region, southern Red Sea, Proc. Indian Acad. Sci. Earth Planet. Sci., 113(3), 269–280,
370 doi:10.1007/BF02716725, 2004.
371 Andersen, O. B. and Knudsen, P.: The role of satellite altimetry in gravity field modelling in
372 coastal areas, Phys. Chem. Earth, Part A Solid Earth Geod., 25(1), 17–24, doi:10.1016/S1464-
373 1895(00)00004-1, 2000.
374 Birol, F., Cancet, M. and Estournel, C.: Aspects of the seasonal variability of the Northern Current
375 (NW Mediterranean Sea) observed by altimetry, J. Mar. Syst., 81(4), 297–311,

376 doi:10.1016/j.jmarsys.2010.01.005, 2010.

377 Bower, A. and Farrar, J. T.: Air – Sea Interaction and Horizontal Circulation in the Red Sea, in

378 The Red Sea the Formation, Morphology, Oceanography and Environment of a Young Ocean

379 Basin, edited by N. M. A. Rasul and I. C. F. Stewart, pp. 329–342, Springer., 2015.

380 Chelton, D. B., Schlax, M. G. and Samelson, R. M.: Progress in Oceanography Global

381 observations of nonlinear mesoscale eddies, Prog. Oceanogr., 91(2), 167–216,

382 doi:10.1016/j.pocean.2011.01.002, 2011.

383 Chelton, U. B., Ries, J. C., Haines, B. J., FU, L.-L. and Callahan, P. S.: Satellite Altimetry and

384 Earth Sciences, in Satellite Altimetry and Earth Sciences A Handbook of Techniques and

385 Applications, edited by L.-L. FU and A. Cazenave, pp. 1–122, Academic Press, San Diego,

386 California ,USA., 2001.

387 Chen, C., Li, R., Pratt, L., Limeburner, R., Berdsley, R., Bower, A., Jiang, H., Abualnaja, Y., Xu,

388 Q., Lin, H., Liu, X., Lan, J. and Kim, T.: Process modeling studies of physical mechanisms of the

389 formation of an anticyclonic eddy in the central Red Sea, J. Geophys. Res. Ocean., 119, 1445–

390 1464, doi:10.1002/2013JC009351, 2014.

391 Clifford, M., Horton, C., Schmitz, J. and Kantha, L. H.: An oceanographic nowcast/forecast system

392 for the Red Sea, J. Geophys. Res. Ocean., 102(C11), 25101–25122, doi:10.1029/97JC01919, 1997.

393 Deng, X. and Featherstone, W. E.: A coastal retracking system for satellite radar altimeter

394 waveforms : Application to ERS-2 around Australia, J. Geophys. Res., 111((C06012)), 1–16,

395 doi:10.1029/2005JC003039, 2006.

396 Deng, X., Featherstone, W. E., Hwang, C. and Shum, C. K.: Improved Coastal Marine Gravity

397 Anomalies at the Taiwan Strait from Altimeter Waveform Retracking, in Proceedings of the

398 International Workshop on Satellite Altimetry for Geodesy, Geophysics and Oceanography.,

399 2001.

400 Desportes, C., Obligis, E. and Eymard, L.: On Wet Tropospheric Correction For Altimetry In

401 Coastal Regions, in 'Envisat Symposium 2007',Montreux, Switzerland, pp. 23–27., 2007.

402 Durand, F., Shankar, D., Birol, F. and Shenoi, S. S. C.: Spatio-temporal structure of the East India

403 Coastal Current from satellite altimetry, J. Geophys. Res. Ocean, 114(2), 18,

404 doi:10.1029/2008JC004807, 2009.

405 Edwards, F. J.: Climate and oceanography, Red sea, 1, 45–68, 1987.

406 Eladawy, A., Nadaoka, K., Negm, A., Abdel-Fattah, S., Hanafy, M. and Shaltout, M.:

Characterization of the northern Red Sea's oceanic features with remote sensing data and outputs from a global circulation model, Oceanologia, 59(3), 213–237, doi:10.1016/j.oceano.2017.01.002, 2017.

Eshel, G. and Naik, N. H.: Climatological Coastal Jet Collision, Intermediate Water Formation, and the General Circulation of the Red Sea, Am. Meteorol. Soc., (1989), 1233–1257, doi:10.1175/1520-0485, 1997.

Ghosh, S., Kumar Thakur, P., Garg, V., Nandy, S., Aggarwal, S., Saha, S. K., Sharma, R. and Bhattacharyya, S.: SARAL/AltiKa Waveform Analysis to Monitor Inland Water Levels: A Case Study of Maithon Reservoir, Jharkhand, India, Mar. Geod., 38(S1), 597–613, doi:10.1080/01490419.2015.1039680, 2015.

Hwang, C., Guo, J., Deng, X., Hsu, H. Y. and Liu, Y.: Coastal gravity anomalies from retracked Geosat/GM altimetry: Improvement, limitation and the role of airborne gravity data, J. Geod., 80(4), 204–216, doi:10.1007/s00190-006-0052-x, 2006.

Johns, W. E., Jacobs, G. a, Kindle, J. C., Murray, S. P. and Carron, M.: Arabian Marginal Seas and Gulfs Report of a Workshop held at., 2000.

Khaki, M., Forootan, E. and Sharifi, M. A.: Satellite radar altimetry waveform retracking over the Caspian Sea, Int. J. Remote Sens., 35(17), 6329–6356, 2014.

Manasrah, R., Badran, M., Lass, H. U. and Fennel, W.: Circulation and winter deep-water formation in the northern Red Sea, Oceanologia, 46(1), 5–23, 2004.

Manasrah, R., Hasanean, H. M. and Al-Rousan, S.: Spatial and seasonal variations of sea level in the Red Sea, 1958-2001, Ocean Sci. J., 44(3), 145–159, doi:10.1007/s12601-009-0013-4, 2009.

Mantripp, D.: Radar altimetry, in The Determination of Geophysical Parameters From Space, edited by N. . Fancey, I. . Gardiner, and R. A. Vaughan, p. 119, Institute of Physics Publishing, London, UK., 1966.

Morcos, S. A.: Physical and chemical oceanography of the Red Sea, Ocean. Mar. Biol. Ann. Rev, 8, 73–202, 1970.

Murray, S. P. and Johns, W.: Direct observations of seasonal exchange through the Bab el Mandab Strait, Geophys. Res. Lett., 24(21), 2557–2560, 1997.

Neumann, A. C. and McGill, D. A.: Circulation of the Red Sea in early summer, Deep Sea Res., 8(3–4), 223–235, 1961.

Osman, M.: Evaporation from coastal water off Port-Sudan, J. King Abdulaziz Univ. Mar. Sci.,

438   17(4), 1–2, 1985.

439   Papadopoulos, V. P., Zhan, P., Sofianos, S. S., Raitsos, D. E., Qurban, M., Abualnaja, Y., Bower,

440   A., Kontoyiannis, H., Pavlidou, A. and Asharaf, T. T. M.: Factors governing the deep ventilation

441   of the Red Sea, J. Geophys. Res. Ocean., 120(11), 7493–7505, 2015.

442   Patzert, W. C.: Wind-induced reversal in Red Sea circulation, Deep Sea Res. Oceanogr., 21(2),

443   109–121, 1974.

444   Phillips, O. M.: On turbulent convection currents and the circulation of the Red Sea, Deep Sea

445   Res., 13(6), 1149–1160, 1966.

446   Quadfasel, D. and Baudner, H.: Gyre-scale circulation cells in the Red-Sea, Oceanol. Acta, 16(3),

447   221–229, 1993.

448   Schmidt, M., Devey, C. and Eisenhauer, A.: FS Poseidon Fahrtbericht/Cruise Report P408

449   [POS408]-The Jeddah Transect; Jeddah-Jeddah, Saudi Arabia, 13.01.-02.03. 2011.

450   Siedler, G.: General circulation of water masses in the Red Sea, in Hot Brines and Recent Heavy

451   Metal Deposits in the Red Sea, edited by E. T. DEGENS and D. A. Ross, pp. 131–137, Springer-

452   Verlag, New York., 1969.

453   Smeed, D. A.: Exchange through the Bab el Mandab, Deep Sea Res. Part II Top. Stud. Oceanogr.,

454   51(4), 455–474, 2004.

455   Sofianos, S. and Johns, W. E.: Water mass formation, overturning circulation, and the exchange

456   of the Red Sea with the adjacent basins, in The Red Sea the Formation, Morphology,

457   Oceanography and Environment of a Young Ocean Basin, edited by N. M. A. Rasul and I. C. F.

458   Stewart, pp. 343–353, Springer., 2015.

459   Sofianos, S. S.: An Oceanic General Circulation Model (OGCM) investigation of the Red Sea

460   circulation: 2. Three-dimensional circulation in the Red Sea, J. Geophys. Res., 108(C3), 3066,

461   doi:10.1029/2001JC001185, 2003.

462   Sofianos, S. S. and Johns, W. E.: An Oceanic General Circulation Model (OGCM) investigation

463   of the Red Sea circulation, 1. Exchange between the Red Sea and the Indian Ocean, J. Geophys.

464   Res., 107(C11), 3196, doi:10.1029/2001JC001184, 2002.

465   Sofianos, S. S. and Johns, W. E.: Observations of the summer Red Sea circulation, J. Geophys.

466   Res., 112, 1–20, doi:10.1029/2006JC003886, 2007.

467   Sofianos, S. S. and Johns, W. E.: Wind induced sea level variability in the Red Sea, Geophys. Res.

468   Lett., 28(16), 3175–3178, 2001.

469 Sultan, S. A. R. and Elghribi, N. M.: Sea level changes in the central part of the Red Sea, Indian J.
470 Mar. Sci., 32(2), 114–122, 2003.

471 Sultan, S. A. R., Ahmad, F. and Nassar, D.: Relative contribution of external sources of mean sea-
472 level variations at Port Sudan, Red Sea, Estuar. Coast. Shelf Sci., 42(1), 19–30, 1996.

473 Taqi, A. M., Al-Subhi, A. M. and Alsaafani, M. A.: Extension of Satellite Altimetry Jason-2 Sea
474 Level Anomalies Towards the Red Sea Coast Using Polynomial Harmonic Techniques, Mar.
475 Geod., doi:10.1080/01490419.2017.1333549, 2017.

476 Tragou, E. and Garrett, C.: The shallow thermohaline circulation of the Red Sea, Deep Sea Res.
477 Part I Oceanogr. Res. Pap., 44(8), 1355–1376, 1997.

478 Vignudelli, S., Cipollini, P., Astraldi, M., Gasparini, G. P. and Manzella, G.: Integrated use of
479 altimeter and in situ data for understanding the water exchanges between the Tyrrhenian and
480 Ligurian Seas, J. Geophys. Res., 105(C8), 19649–19664, doi:10.1029/2000JC900083, 2000.

481 Vignudelli, S., Cipollini, P., Roblou, L., Lyard, F., Gasparini, G. P., Manzella, G. and Astraldi,
482 M.: Improved satellite altimetry in coastal systems : Case study of the Corsica Channel (
483 Mediterranean Sea), Geophys. Res. Lett., 32(L07608), 1–5, doi:10.1029/2005GL022602, 2005.

484 Yao, F., Hoteit, I., Pratt, L. J., Bower, A. S., Zhai, P., Kohl, A. and Gopalakrishnan, G.: Seasonal
485 overturning circulation in the Red Sea: 1. Model validation and summer circulation, J. Geophys.
486 Res. Ocean., 119, 2238–2262, doi:10.1002/2013JC009331.Key, 2014a.

487 Yao, F., Hoteit, I., Pratt, L. J., Bower, A. S., Köhl, A., Gopalakrishnan, G. and Rivas, D.: Seasonal
488 overturning circulation in the Red Sea: 2. Winter circulation, J. Geophys. Res. Ocean., 119(4),
489 2263–2289, doi:10.1002/2013JC009331, 2014b.

490 Zhan, P., Subramanian, A. C., Yao, F. and Hoteit, I.: Eddies in the Red Sea: A statistical and
491 dynamical study. Geophys. Res. Ocean., 119, 3909–3925, doi:10.1002/2013JC009563, 2014.

492
493

494
495